

Article

The GPM Validation Network and Evaluation of Satellite-Based Retrievals of the Rain Drop Size Distribution

Patrick N. Gatlin ^{1,*}, Walter A. Petersen ¹, Jason L. Pippitt ², Todd A. Berendes ³, David B. Wolff ⁴ and Ali Tokay ⁵

¹ NASA Marshall Space Flight Center, Huntsville, AL 35812, USA; walt.petersen@nasa.gov

² Science Systems and Applications, Incorporated/NASA Goddard Space Flight Center, Greenbelt, MD 20771, USA; jason.l.pippitt@nasa.gov

³ Earth Systems Science Center/NASA Marshall Space Flight Center, University of Alabama in Huntsville, Huntsville, AL 35805, USA; todd.a.berendes@nasa.gov

⁴ Wallops Flight Facility, NASA Goddard Space Flight Center, Wallops, VA 23337, USA; david.b.wolff@nasa.gov

⁵ Joint Center for Earth Systems Technology/NASA Goddard Space Flight Center, University of Maryland Baltimore County, Greenbelt, MD 20771, USA; ali.tokay-1@nasa.gov

* Correspondence: patrick.gatlin@nasa.gov; Tel.: +1-256-961-9710

Received: 20 August 2020; Accepted: 11 September 2020; Published: 21 September 2020



Abstract: A unique capability of the Global Precipitation Measurement (GPM) mission is its ability to better estimate the raindrop size distribution (DSD) on a global scale. To validate the GPM DSD retrievals, a network of more than 100 ground-based polarimetric radars from across the globe are utilized within the broader context of the GPM Validation Network (VN) processing architecture. The GPM VN ensures quality controlled dual-polarimetric radar moments for use in providing reference estimates of the DSD. The VN DSD estimates are carefully geometrically matched with the GPM core satellite measurements for evaluation of the GPM algorithms. We use the GPM VN to compare the DSD retrievals from the GPM's Dual-frequency Precipitation Radar (DPR) and combined DPR–GPM Microwave Imager (GMI) Level-2 algorithms. Results suggested that the Version 06A GPM core satellite algorithms provide estimates of the mass-weighted mean diameter (D_m) that are biased 0.2 mm too large when considered across all precipitation types. In convective precipitation, the algorithms tend to overestimate D_m by 0.5–0.6 mm, leading the DPR algorithm to underestimate the normalized DSD intercept parameter (N_w) by a factor of two, and introduce a significant bias to the DPR retrievals of rainfall rate for DSDs with large D_m . The GPM Combined algorithm performs better than the DPR algorithm in convection but provides a severely limited range of N_w estimates, highlighting the need to broaden its a priori database in convective precipitation.

Keywords: precipitation; remote sensing; microphysics

1. Introduction

Understanding the distribution of precipitation is vital to gaining new insights into the water and energy cycle of the Earth system and how this life-essential resource evolves in a changing climate. Hence, accurate precipitation estimates are required on a global scale—something only possible with Earth observing satellites. The Global Precipitation Measurement (GPM) mission provides these observations using a core satellite, which consists of the Dual-frequency Precipitation Radar (DPR) and the GPM Microwave Imager (GMI), operating within and calibrating a constellation of microwave radiometers [1,2]. Building upon the 17 years of satellite-based observations from the Tropical Rainfall

Measurement (TRMM) mission [3,4], the GPM extends the precipitation program of record to higher latitudes and facilitates new satellite-based measurements of raindrop size, which improves the retrieved rainfall estimate. One of the science requirements for the GPM core satellite is to provide an estimate of raindrop sizes accurate to within 0.5 mm. This retrieval is largely facilitated by DPR's ability to obtain radar measurements at two different frequencies—the Ku-(13.6 GHz) and Ka-band (35 GHz), whose differential scattering in rain is directly related to the size of the raindrops [5,6]. However, validating this on a global scale is not a trivial task, especially since the sampling area of disdrometers does not exceed 100 cm².

Ground-based polarimetric weather radars have been used for decades to obtain rather accurate estimates of precipitation [7–10]. This is enabled through the polarimetric radar's capability to sample precipitation using two orthogonal signals that provide a direct measure of the size of raindrops as well as information about hydrometeor characteristics [11]. Numerous studies have demonstrated that the median or mass-weighted mean raindrop diameters (D_o and D_m , respectively) can be retrieved from polarimetric radar measurements within $\pm 10\%$ of that measured by a disdrometer [12–14]. In addition to retrieving the characteristic size of raindrops, application of a rain drop size distribution (DSD) model, such as the widely used gamma probability distribution function [15,16], also facilitates retrieval of the number concentration of raindrops. Such radar-based retrieval algorithms are commonly derived from disdrometer measurements [11,13,17].

The strategy used in GPM ground validation (GV) is a multi-faceted direct approach that uses a myriad of precipitation instruments, including disdrometers and polarimetric radars, to assess the performance of precipitation products from the GPM core satellite [18]. The objective is to translate high quality precipitation measurements collected at very fine scales (0.1 km) to the much larger footprint scale of the satellite (4–50 km resolution over swaths spanning 100–1000 km). To obtain these multi-scale reference measurements, NASA GV has deployed these instruments in multiple field campaigns [19–23] and to collect long-term statistics at strategic sites with existing complimentary infrastructure [18,24]. The GPM retrieval algorithms are still undergoing improvements and revision. Hence ongoing validation is required without the luxury of data-rich, yet costly field campaigns. The GPM Validation Network (VN) is GV's solution to continue assessing the accuracy of the satellite-based precipitation estimates with each new version of the GPM retrieval algorithms. A prototype of the VN was developed by [25] using the TRMM Precipitation Radar and 25 ground-based weather radars, but it was focused mainly on comparing radar reflectivity and rainfall rate. Since the launch of GPM in 2014, the VN has been greatly expanded to include over 100 ground-based radars, including numerous international dataset contributions [18], and enhanced with additional information content facilitated by the multitude of precipitation measurements collected in GPM GV field campaigns and related efforts.

The purpose of this paper is to describe polarimetric radar-based enhancements to the GPM Validation Network (VN) processing architecture that have occurred during the GPM-era, and how the VN is used to validate the precipitation retrievals from the DPR and GMI measurements, focusing on retrieval of the DSD. In Section 2, we provide an overview of the VN architecture including how disdrometers and polarimetric radars are used to obtain a reference measurement of the DSD, and subsequent geometric matching to the associated GPM satellite-based estimates. Example comparisons between the ground-based retrievals and GPM for different types of rainfall are presented in Section 3 with a discussion, summary and conclusion following in Sections 4 and 5.

2. Data and Methods

The VN is a software system whose primary function is to facilitate comparison of precipitation retrievals from the GPM core satellite measurements with those obtained from ground-based polarimetric radars. The current version of the VN consists of observations from 118 ground-based radars spanning diverse geographical regions and meteorological regimes (Figure 1). The GPM-era VN database extends backward to March 2014, just after the launch of the GPM core satellite. In addition to the standard radar-based variables (e.g., reflectivity), the VN provides geophysical variables (e.g., DSD,

rainfall rate) derived from more than 400,000 min of two-dimensional video disdrometer measurements in the following regions: southern Finland; central Oklahoma; southern Ontario, Canada; eastern Iowa; western North Carolina, Olympic Peninsula; Huntsville, Alabama; Wallops Island, Virginia [17]. Hence the VN database serves the GPM mission as the connection between the disdrometer observations and the satellite-based DSD retrievals.

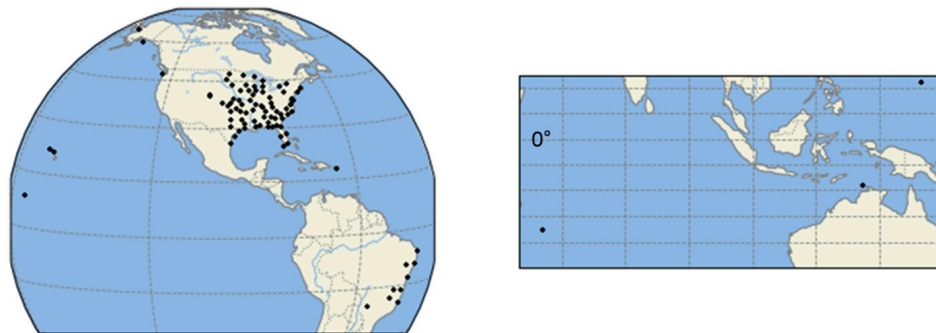


Figure 1. Map of ground-based radar (GR) sites that are ingested by the Global Precipitation Measurement (GPM) Validation Network (VN).

The VN ingests ground-based polarimetric radar data from a variety of sources, including both operational and research weather radars, processes the raw radar moment data to obtain geophysical variables and geometrically matches those with DPR and the GMI retrievals during GPM core satellite overpasses within 100-km of each radar ingested. A schematic of this workflow is given in Figure 2.

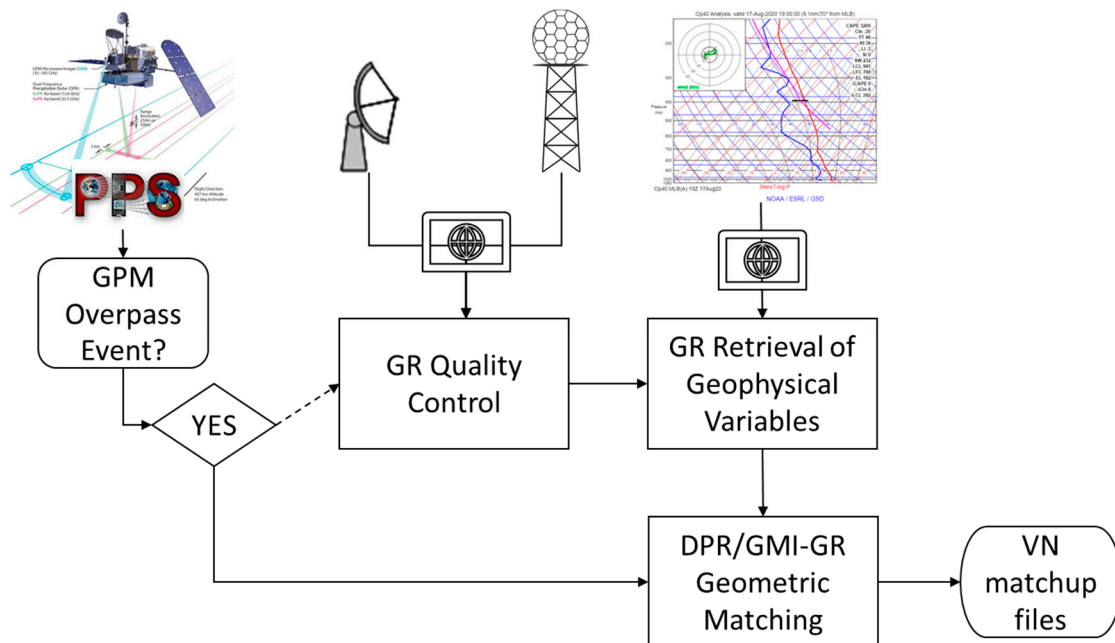


Figure 2. Workflow of the GPM VN process to produce Dual-frequency Precipitation Radar (DPR)/GPM Microwave Imager (GMI)-GR matchup files.

2.1. Data Sources

Operational radar datasets such as National Oceanic and Atmospheric Administration (NOAA) National Weather Service WSR-88D Level II radar data are acquired in near real time from NOAA’s publicly accessible archive hosted on the Amazon Web Services Simple Storage Solution cloud platform [26]. Across the continental United States (CONUS), the VN includes most polarimetric Weather Surveillance Radar, 1988, Doppler radars (WSR-88Ds) east of the Rocky Mountains. This region

is selected in a somewhat conservative fashion as a zeroth order approach to maximize GV reference data quality by avoiding radar observations affected by terrain blockage and associated clutter, while at the same time optimizing the associated sampling range/area of the given radars underneath periodic overpasses of the GPM core satellite. Beyond this initial selection of radars, WSR-88Ds in Alaska, Hawaii, Guam and Puerto Rico are now also processed. This equates to nearly 200 GB of WSR-88Ds data ingested by the VN each day. In addition to the network of WSR-88D radars, the VN also routinely ingests S-band polarimetric radar data from Brazil's Center for Monitoring and Alerting of Natural Disasters (CEMADEN) radar network, and radar data from the Kwajalein Polarimetric S-band Weather Radar (KPOL) [27], which is located in the Central Pacific. Radars primarily used for research are also ingested by the VN but less frequently pending their operations and timing of GPM overpasses. These include the following polarimetric radars: the NASA Polarimetric Doppler Weather Radar (NPOL) [28]; the Colorado State University–University of Chicago–Illinois State Water Survey (CSU–CHILL) [29]; the University of Alabama in Huntsville/WHNT-TV Advanced Radar for Meteorological and Operational Research (ARMOR) [30]; the C-band polarimetric/Doppler meteorological radar system (C-POL) in Darwin, Australia [31]. The VN also includes data from Météo-France's S-band polarimetric radar at Piton Villers on La Réunion [32] collected between 2014 and 2017, providing a unique site in the southern Indian Ocean to enrich GPM GV.

The VN routinely ingests atmospheric sounding information from the National Oceanic and Atmospheric Administration (NOAA) Rapid Refresh (RAP) hourly model analysis [33], the Global Forecast System [34], the Flow-Following, Finite Volume Icosahedral Model [35] and from radiosondes launched daily at Kwajalein Atoll to extract vertical temperature and moisture profiles used in the VN hydrometeor identification (HID) scheme [36], whose weights have been adjusted for S-band. Additionally, the GPM Precipitation Processing System [37] provides orbital subsets of the GPM products for each ground radar ingested by the VN. When a GPM overpass occurs within 200-km of a given radar, the VN ground radar (GR) processing is activated. Approximately 40 GPM overpasses occur over VN radars daily. The GR processing is largely automated, except for occasional manual checks to ensure only valid precipitation events are included in the database. Since the VN must process radar data from a variety of different radar platforms, the VN software includes data readers to handle each of the various radar data formats (e.g., netCDF, Archive Level-II, SIGMET, Rainbow).

2.2. GR Data Processing

Each GR data set is put through automated and manual quality control (QC). First, NASA's Dual Polarimetric Quality Control (DPQC) algorithm is used to identify and remove non-precipitation echoes [38]. If any unwanted echoes remain, the QC algorithm's polarimetric thresholds are manually adjusted and the data is processed through it again [38]. This iterative QC procedure continues until the GR data are deemed acceptable (i.e., a trained operator does not find any remaining clutter or other non-precipitation echoes). Most of the GR datasets ingested by the VN are from operational networks, which typically have routine maintenance schedules, hence, routine calibration is checked only for NPOL and KPOL reflectivity and differential reflectivity data. For these non-operational radars, the VN uses the Relative Calibration Adjustment technique [39,40], self-consistency of polarimetric variables [41], and vertical profile (or birdbath) scans [42]. While occasional manual verification of operational radar datasets is undertaken, for the large operational radar datasets such as the WSR-88Ds it is more generally assumed that the large statistical data-base approach relying on tens of thousands or more data points and extended duration will provide an unbiased reference comparison with an varied degree of random error (which will be apparent in following figures). This, as it is highly unlikely that systematic bias will (a) remain at any single radar for multiple years; or, (b) exist uniformly in the entire data sample of 100+ radars at any given time over multiple years. We are able to approximately validate this assumption using time-series comparisons of GPM DPR radar reflectivity aloft in stratiform regions where ice dominates. The time series comparisons show occasional negative and positive departures of GR calibration relative to the GPM, but the departures often oscillate with ± 2 dB of the GPM

radar values. We assume this is also the case for biases in polarimetric moments, and with subsequent application in large numbers of samples to ensure that our comparisons to GPM will be dominated primarily by random error and only minimal bias (i.e., much less than requirements dictate [18]).

An additional step related to GR data quality is the computation of specific differential phase (K_{dp}), which is used for attenuation correction and rainfall estimation. The VN uses an adaptive K_{dp} estimation algorithm developed by [43] to extract the differential propagation phase shift from the total differential phase measured at each range gate along the radar ray and estimate the K_{dp} . Although many of the GR datasets already contain an estimate of K_{dp} when ingested by the VN, this new K_{dp} is used instead.

2.3. GR-Based Retrievals of the DSD

The processed (i.e., QC, attenuation corrected) GR data are used to retrieve, amongst other geophysical variables (e.g., rainfall rate), two parameters of the normalized gamma DSD model— D_m , which is defined as the ratio of the fourth to the third moment of the DSD, and the normalized intercept parameter, N_w [11]. The retrieval is derived from T-matrix scattering simulations performed using a very large (>300,000 min of DSDs) and diverse database of optical disdrometer observations collected for GPM GV efforts [17]. Using a third-order polynomial with a sequential intensity filtering technique [44], the D_m is retrieved from the GR observed differential reflectivity, Z_{dr} , (after QC and attenuation correction) and used together with the GR observed radar reflectivity (i.e., Z_h after QC and attenuation correction) to retrieve N_w . The DSD model-fit of the “ALL campaign” described by [17] produces a relative bias of less than 10% and a relative mean absolute error of less than 15% near the ground. Further details of this retrieval process, including the relevant equations, are found in [17]. It is worth noting here that the level 2 radar data the VN obtains from the WSR-88D network includes an internal Z_{DR} bias correction, which is monitored by the National Weather Service Radar Operations Center and found to be within 0.2 dB [45]. Additionally, we examined the VN data used in this study and found the Z_{DR} bias to be 0.06 dB for drizzle (as identified by the polarimetric hydrometeor classification) and the reflectivity is 15–23 dBz. Hence, a Z_{DR} bias does not significantly impact the DSD retrievals from the ground-based radars presented in this study.

2.4. GPM Core Satellite-Based Retrievals of the DSD

The VN includes observations and retrievals from both the DPR and GMI. The GPM/DPR Level 2 algorithm (2ADPR; [46]) uses single and dual frequency measurements from the DPR to retrieve the DSD. Its approach relies on the relationship between rain rate, R , and D_m , and performs a path-integrated attenuation-constrained optimization to find a unique R – D_m relation for each precipitation type with N_w following from the resultant optimal solution of D_m and R [47]. The Level 2B GPM Combined Radar–Radiometer Precipitation Algorithm (2BCMB) uses both the Level 2 calibrated reflectivity profiles from the DPR and Level 1C GMI brightness temperatures together with an a priori database of particle size distributions and corresponding environmental conditions to retrieve the DSD and other integral rain parameters [48]. It begins with an initial guess of N_w profiles based on the a priori database in relation to the satellite observations and employs an ensemble filter within an optimal estimation framework to find the most likely profile of N_w and D_m [49].

2.5. Matching the Satellite and GR Retrievals

The ground radar (GR) and DPR observe the precipitation from different perspectives and at different resolutions. The DPR has a swath of 245-km with a nadir pixel level footprint of 5-km in diameter and vertical resolution of 250-m. A typical GR has 125–250 m range gate spacing (depending on whether it is a research or operational radar) and 3 dB beam width of 1° , giving it better horizontal resolution than DPR. Hence, the VN applies a geometrical matching of the GR bins for intersecting DPR rays. A thorough discussion on the specifics of the geometrical matching procedure is provided in [25]. So here we just give an example of this for a single DPR ray (Figure 3). To capture the precipitation

variability within any given DPR footprint, the VN computes statistics (e.g., mean, median, standard deviation, maximum) of the GR fields at each GR elevation angle intersecting each DPR ray within the GR domain. For the HID field, the GR bins assigned to each HID class at each GR elevation angle intersecting a DPR ray are summed for each class (i.e., histogram of HID). In addition, for each GR elevation angle, the DPR bins are averaged within each intersecting GR ray. These geometrically matched data are stored in netCDF formatted files and archived (see supplemental material for data location online). Matchup files exist for each version of 2ADPR and 2BCMB during GPM overpasses of GR sites when precipitation was detected by the satellite. In this study, we include VN matchups for six years of Version 06A GPM algorithms from 2014 through 2019.

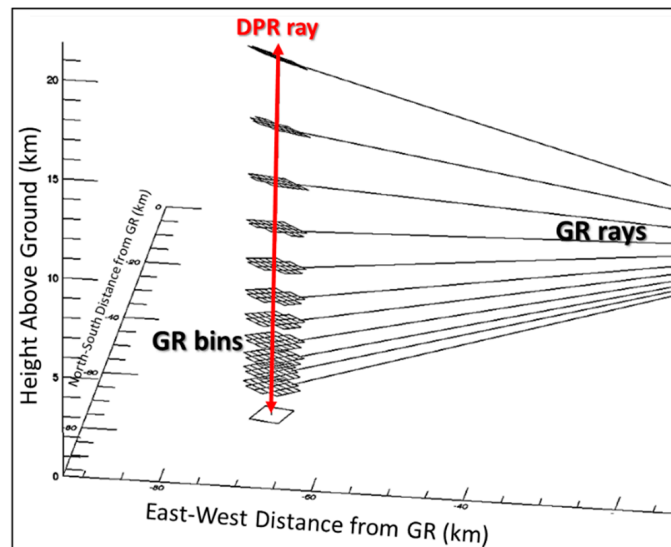


Figure 3. An illustration of the geometrical matching between the satellite DPR and ground-based radar (GR) rays.

3. Results

In this section, we present comparisons of the DSD retrievals (1-km below the melting layer) from 2ADPR and 2BCMB with those from the CONUS ground-based radars (GRs) in the GPM VN matchup archive. The focus is on evaluating the performance of the GPM algorithms and using the VN to help diagnose sources of error. Figure 4 shows the retrievals of D_m from Version 06A of 2ADPR and 2BCMB for stratiform and convective rainfall, which is based on the precipitation type classification of 2ADPR [46]. Note that, in contrast to that discussed in [17], this comparison focuses on a new algorithm version (V06A) and significantly extends the time period of comparisons (and hence sample numbers). It includes 319,063 (116,218) matchups of D_m retrievals from 2ADPR (2BCMB) for the DPR matched scans (i.e., the Ku-band and Ka-band scans) within its inner swath (2BCMB also includes GMI observations). Both GPM algorithms produce a larger D_m than that of the GR as in Petersen et al. (2020), with 2BCMB exhibiting a 0.2 mm high bias and 2ADPR exhibiting a slightly lower mean absolute error (MAE), particularly in stratiform precipitation (Figure 4a). However, in convective precipitation the MAE of the 2ADPR D_m retrieval is 0.5 mm, whereas 2BCMB has the lower error. Furthermore, the GPM retrievals of convective precipitation exhibit peculiar behavior at large D_m (>2.5 mm), especially 2ADPR (Figure 4c). In Figure 4c, the GPM retrievals appear to saturate around 3.0 mm, but this is an artifact of the matched scan (MS) in which Ka-band retrieval of D_m is limited to <3.0 mm. The 2AKu retrieval (i.e., Ku-band only) of D_m does not exhibit such artificial behavior, but like Figure 4c, it does increasingly depart in a marked positive bias fashion from agreement with the ground radars (not shown). Although the GPM retrieval of D_m meets the mission level 1 requirements of being within ± 0.5 mm [50], which is largely due to its superb performance in stratiform

precipitation, the V06 DPR algorithms clearly exhibit departures from the GR retrievals of D_m within convective precipitation.

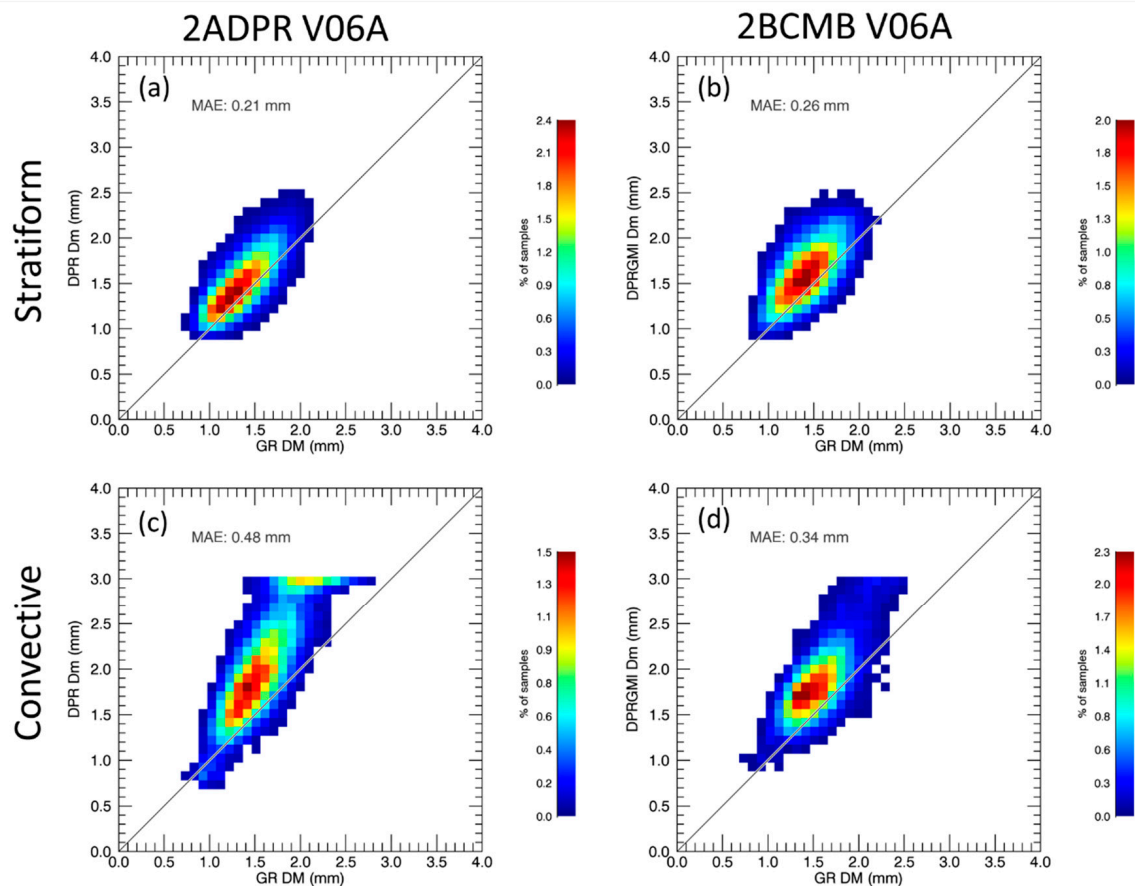


Figure 4. A VN-based comparison of mass-weighted mean diameter (D_m) retrievals for the GPM core satellite and the GR for (a,b) stratiform and (c,d) convective precipitation for Version 06A of the (a,c) GPM/DPR Level 2 (2ADPR) and (b,d) Level 2B GPM Combined Radar–Radiometer Precipitation (2BCMB) GPM algorithms.

As previously discussed, disdrometer measurements across the globe and a variety of precipitation types represent the foundation of the DSD retrievals in the VN. Indeed, Figure 5a demonstrates that DSD retrievals by ground radars (GRs) included in the VN database agree quite well with observations from a global disdrometer-based DSD dataset [51]. The DPR retrievals are offset relative to the GR (Figure 5b,c). In addition to the high bias in D_m , the DPR retrievals tend to have significantly lower N_w —an order of magnitude for 2AKu (Figure 5b). The DSD bias is less severe for the dual-frequency retrieval, but the upper constraint on D_m from the Ka-band information is readily apparent (Figure 5c). However, in precipitation classified as convective by 2ADPR, the GR D_m retrievals are shifted approximately 0.3 mm lower than the global DSD observations classified by [51] as being associated with convective precipitation processes (i.e., their Groups 1,3,5, and 6). In fact, both the GR and DPR median D_m retrievals are within 0.2 mm of the observed DSDs classified as convective. The GR retrievals of N_w for convective precipitation are nearly spot on with that observed (Figure 5a), but the DPR algorithms have a problem with the retrieval of N_w in convective precipitation. In stratiform precipitation, the DPR retrievals of N_w are within $\pm 15\%$ of the GR retrieved N_w (not shown).

Figure 6 shows the 2BCMB and 2ADPR retrievals of N_w relative to the GR within the inner swath of the DPR. The behavior is markedly different between the two algorithms. The correlation between the GR and 2BCMB retrievals of N_w is very weak compared to that of the GR and 2ADPR estimates. The DPR retrievals of N_w extend across three orders of magnitude, which is similar to the dynamic

range of the GR retrievals, but the 2BCMB retrievals of N_w range less than two orders of magnitude. This is especially the case for convective precipitation. The 2BCMB retrievals of $\log_{10}(N_w)$ are largely concentrated around 3.5 (Figure 6d), and this represents a strong a priori database constraint on N_w retrievals in the 2BCMB algorithm. The low bias of 2ADPR estimates of N_w in convection (Figure 6c) are reflective of the its high bias in D_m (Figure 4c).

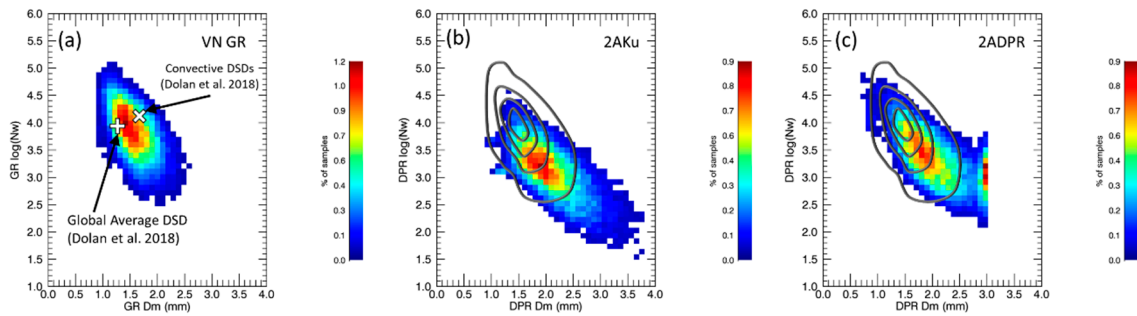


Figure 5. Convective rain drop size distribution (DSD) retrievals within the DPR matched scan (MS)/inner swath from (a) the GRs, and from DPR’s (b) 2AKu (single frequency), and (c) 2ADPR (dual frequency) Version 06A algorithms. The “+” and “X” in (a) are the average D_m and normalized intercept parameter (N_w) of the Global and convective DSDs, respectively, presented in Dolan et al. (2018). The contour lines in (b,c) mimic the pattern of the GR distribution in (a). The N_w used in $\log_{10}(N_w)$ is normalized by $1 \text{ m}^{-3}\text{mm}^{-1}$.

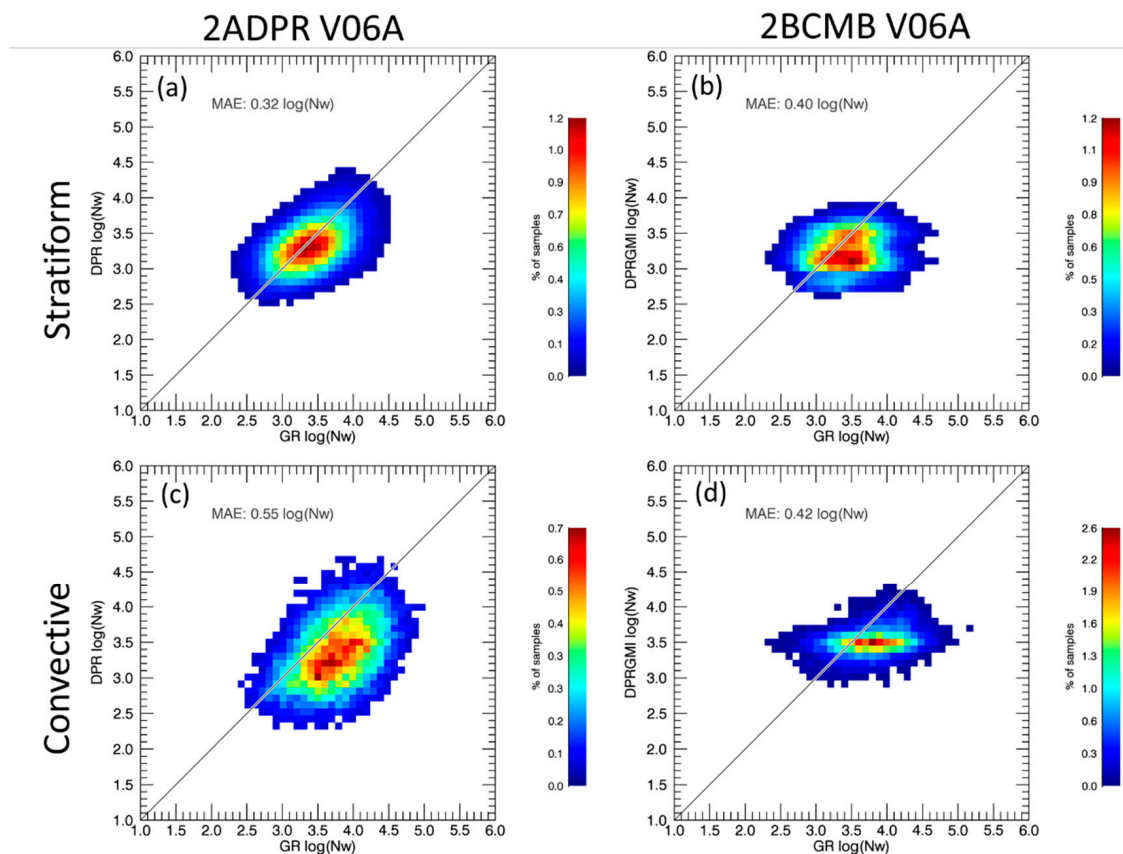


Figure 6. The retrievals of $\log_{10}(N_w)$ from (left) 2ADPR and (right) 2BCMB relative to the GRs in (a,b) stratiform and (c,d) convective precipitation within the DPR inner (MS) swath.

4. Discussion

We have identified a few issues with the DSD retrievals from the GPM V06A algorithms, predominately in convective rain. In this section, we will further discuss them and utilize the GR data included in the VN to shed some light on potential sources of these errors.

For DSDs comprised of a relatively high number of large raindrops (e.g., $D_m > 2.5$ mm), the 2ADPR retrievals of D_m become increasingly positive biased relative to GR retrieved D_m , primarily for convective precipitation (Figure 4). Using the polarimetric radar retrievals of hydrometeor type (i.e., HID), we find relatively more rimed ice aloft (e.g., graupel and hail) when 2ADPR retrievals of $D_m > 2.5$ mm occur within convective precipitation (Figure 7). The presence of larger ice particles such as graupel and hail and associated potential mixed phase conditions, is consistent with the presence of larger drops and a modest positive shift in D_m [51,52]. However, these conditions can also produce non-uniform beam filling and multiple scattering at the Ku- and, especially, Ka-bands, thereby complicating the attenuation correction of the DPR [53]. The 2BCMB algorithm includes a solution for handling multiple scattering at the Ka-band [48], which may be a reason for it being slightly less biased at large D_m than 2ADPR is in convective precipitation. However, the 2BCMB retrievals of D_m still exhibit an increasing bias with $D_m > 2.5$ mm, suggesting it may not be fully accounting for the effects of multiple scattering and/or non-uniform beam filling (NUBF), which can also affect the satellite retrievals in deep convection [54].

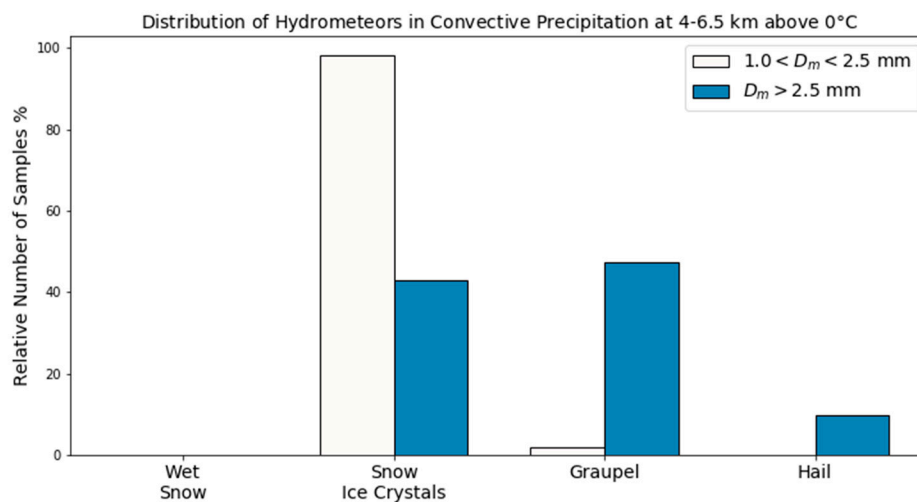


Figure 7. VN matchups of GR hydrometeor identifications at 4–6.5 km above 0 °C within DPR inner swath rays through convective precipitation in which 2ADPR retrievals are (white) $1.0 < D_m < 2.5$ mm and (filled) $D_m > 2.5$ mm.

In GPM DPR algorithm retrievals of rain rate, the R – D_m relationship is a dominant player [55]. Moreover, recall that when the D_m bias gets large in the DPR estimates, that $\log_{10}(N_w)$ is observed to become markedly lower relative to both the VN and ground-based disdrometer measurements (Figure 5). Collectively, this results in an underestimation of rain rate for similar radar reflectivity. Indeed, the impact of a positive bias in the D_m retrievals for the GPM algorithms is readily observed in comparisons of rainfall rate to VN estimates. For example, if convective rainfall rates associated with large D_m in the outer swath of the DPR (i.e., Ku-only measurements) are extracted from the rain rate sample, and then compared to the VN polarimetric radar-based rainfall rates [10], the effect of large D_m on the rain rate bias is removed (Figure 8).

Reasons for the bias in D_m are not clear. However, in a NUBF situation (more likely to occur in convective precipitation) it is conceivable that measured attenuation at a lower reflectivity value (due to the NUBF) could be over compensated by an increase in the initial D_m estimate via the R – D_m approach, which would drive down N_w and the rainfall rate.

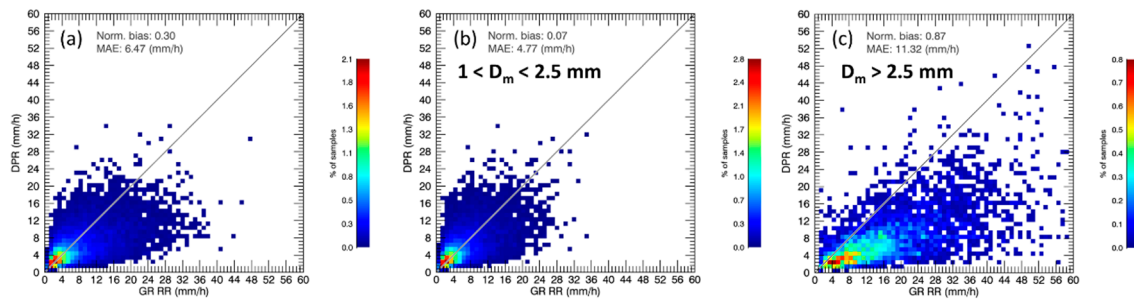


Figure 8. VN comparison of rainfall rate retrieved from 2ADPR within the outer swath scans of the DPR within (a) convective precipitation and convective precipitation (b) without large D_m and (c) with only large D_m .

The GPM retrievals of N_w are significantly biased low. The 2ADPR approach to retrieving N_w is similar to that used with the GR in that it is dependent upon D_m and reflectivity, Z . However, 2ADPR assumes a fixed shape parameter in the gamma DSD (i.e., $\mu = 3$) and includes an adjustment factor, ϵ , that defines the R - D_m , which is used to estimate D_m , and the Z - D_m relationship, which is then used to estimate N_w . A robust description of 2ADPR's DSD retrieval approach is provided in [56]. The ϵ is optimally determined from the forward (i.e., downward starting at the storm top) recursively estimated attenuation versus that observed via the surface-reference technique [47,55]. Since an inherent inverse relationship exists between N_w and D_m (e.g., Figure 5), retrieval approaches such as 2ADPR with a high bias in D_m can in turn produce a low bias in N_w . We find severely negatively biased N_w retrievals in convective precipitation, where the D_m estimates are 0.5–0.6 mm too high relative to the GR. The significantly more accurate N_w estimate in stratiform precipitation is in part evidence for the impact of errors in the D_m retrieval on 2ADPR's retrievals of the DSD and ultimately its rainfall estimates. Additional factors may be at play in contributing to 2ADPR's order of magnitude N_w bias in convective precipitation. The optimization approach to find the ϵ used in the 2ADPR DSD retrievals involves simulating the attenuation at the Ka-band, which in convection can suffer from multiple scattering and non-uniform beam filling [54,57]. The assumption of a fixed μ in the formulation of the gamma DSD is certainly another possible source of error, however, it is likely to be of lower impact since μ exhibits little variability over a vast range of D_m and N_w normalized rainfall rates [58].

The 2BCMB estimates of N_w have greater error than 2ADPR, except in convection, which is a testament to the 2BCMB attempt to account for multiple scattering and non-uniform beam filling. However, in convection the 2BCMB tends to often arrive at N_w estimates between 2500 and 3500 $\text{m}^{-3}\text{mm}^{-1}$, which is not realistic and highlights a problem with the algorithm. The 2BCMB DSD retrieval approach differs from 2ADPR in that it first retrieves N_w and then D_m . The 2BCMB relies on a database of N_w profiles that serves as a starting point and constraining a priori distribution for this iterative Bayesian-based approach [49]. Hence the retrievals are only as representative as the a priori database. Therefore, this database may not be representative enough in convective precipitation, causing the optimal estimation used in 2BCMB to often converge on the initial N_w profile.

5. Conclusions

The VN offers detailed insights into the inner workings of the GPM algorithms and can help to pinpoint any deficiencies. In this study, we compared DSD retrievals from 2ADPR and 2BCMB with those from numerous ground-based polarimetric radars. We find that both 2ADPR and 2BCMB estimates of D_m are biased high by only 0.2 mm, thereby meeting the level 1 science requirement. However, the algorithms do not estimate the DSD as well in convective precipitation. They tend to increasingly overestimate D_m when graupel and hail are present in the column of convective precipitation, likely causing multiple scattering at the Ka-band and possibly exacerbating attenuation correction. This is especially true when 2ADPR estimates $D_m > 2.5$ mm, but less so for 2BCMB.

Additionally, the 2AKa upper constraint on D_m artificially limits the 2ADPR retrievals of $D_m < 3.0$ mm within the inner (aka MS) swath and subsequently affects the rain rate retrievals for these large D_m .

The high bias in D_m partially explains the low bias in the N_w retrievals with 2ADPR, and the presence of multiple scattering and non-uniform beam filling are also likely to blame in convective precipitation. Although 2BCMB provides a better estimate of N_w than 2ADPR, its significantly smaller dynamic range highlights the need to broaden its a priori database of convective precipitation and perhaps revisit its optimal estimation approach.

The VN matchup files are available for download from the NASA Distributed Active Archive Center Global Hydrology Resource Center (see Supplementary Materials). Additionally, a recent project is underway to store the VN dataset into an Athena database hosted on Amazon Web Services to enable GV and other users to readily query and extract subsets of the VN dataset [59]. The VN is continually being enhanced as a tool for precipitation science. It now consists of vertical motion retrieved via a multi-Doppler three-dimensional variational (3DVAR) approach [60,61] implemented in the Python Direct Data Assimilation (PyDDA) software package [62] for more than 20 pairs of WSR-88D radars [63]. Hence the VN now facilitates investigation of microphysical and dynamical processes that occur within the GPM satellite footprint—a vital observation to serve the program of record for future satellite missions focused on convective precipitation processes.

Supplementary Materials: The VN matchups used in this study are available online at <http://dx.doi.org/10.5067/GPMGV/WFF/MULTIPLE/DATA101>.

Author Contributions: Conceptualization, W.A.P. and P.N.G.; methodology, W.A.P., T.A.B. and J.L.P., A.T.; software, T.A.B. and J.L.P.; validation, W.A.P. and P.N.G.; formal analysis, P.N.G. and W.A.P.; investigation, W.A.P. and P.N.G.; project administration, D.B.W.; data curation, T.A.B. and J.L.P.; writing—original draft preparation, P.N.G.; writing—review and editing, P.N.G. and W.A.P.; visualization, T.A.B. and P.N.G.; All authors have read and agreed to the published version of the manuscript.

Funding: This research was funded by Gail Skofronick-Jackson of NASA Headquarters as a part of the Global Precipitation Measurement mission Ground Validation.

Acknowledgments: We would like to thank Robert K. Morris for designing the VN software framework.

Conflicts of Interest: The authors declare no conflict of interest. The funders had no role in the design of the study; in the collection, analyses, or interpretation of data; in the writing of the manuscript, or in the decision to publish the results.

References

- Hou, A.Y.; Kakar, R.K.; Neeck, S.; Azarbarzin, A.A.; Kummerow, C.D.; Kojima, M.; Oki, R.; Nakamura, K.; Iguchi, T. The Global Precipitation Measurement Mission. *Bull. Am. Meteorol. Soc.* **2014**, *95*, 701–722. [[CrossRef](#)]
- Skofronick-Jackson, G.; Kirschbaum, D.; Petersen, W.; Huffman, G.; Kidd, C.; Stocker, E.; Kakar, R. The Global Precipitation Measurement (GPM) mission's scientific achievements and societal contributions: reviewing four years of advanced rain and snow observations. *Q. J. R. Meteorol. Soc.* **2018**. [[CrossRef](#)] [[PubMed](#)]
- Simpson, J.; Kummerow, C.; Tao, W.-K.; Adler, R.F. On the Tropical Rainfall Measuring Mission (TRMM). *Meteorol. Atmos. Phys.* **1996**, *60*, 19–36. [[CrossRef](#)]
- Kummerow, C.; Barnes, W.; Kozu, T.; Shiue, J.; Simpson, J. The Tropical Rainfall Measuring Mission (TRMM) Sensor Package. *J. Atmos. Ocean. Technol.* **1998**, *15*, 809–817. [[CrossRef](#)]
- Mardiana, R.; Iguchi, T.; Takahashi, N. A dual-frequency rain profiling method without the use of a surface reference technique. *IEEE Trans. Geosci. Remote Sens.* **2004**, *42*, 2214–2225. [[CrossRef](#)]
- Liao, L.; Meneghini, R. A study of air/space-borne dual-wavelength radar for estimation of rain profiles. *Adv. Atmos. Sci.* **2005**, *22*, 841–851. [[CrossRef](#)]
- Seliga, T.A.; Bringi, V.N. Differential reflectivity and differential phase shift: Applications in radar meteorology. *Radio Sci.* **1978**, *13*, 271–275. [[CrossRef](#)]
- Bringi, V.N.; Chandrasekar, V.; Balakrishnan, N.; Zrnić, D.S. An {Examination} of {Propagation} {Effects} in {Rainfall} on {Radar} {Measurements} at {Microwave} {Frequencies}. *J. Atmos. Ocean. Technol.* **1990**, *7*, 829–840. [[CrossRef](#)]

9. Ryzhkov, A.V.; Schuur, T.J.; Burgess, D.W.; Heinselman, P.L.; Giangrande, S.E.; Zrnica, D.S. The Joint Polarization Experiment: Polarimetric rainfall measurements and hydrometeor classification. *Bull. Am. Meteorol. Soc.* **2005**, *86*, 809–824. [[CrossRef](#)]
10. Cifelli, R.; Chandrasekar, V.; Lim, S.; Kennedy, P.C.; Wang, Y.; Rutledge, S.A. A New Dual-Polarization Radar Rainfall Algorithm: Application in Colorado Precipitation Events. *J. Atmos. Ocean. Technol.* **2011**, *28*, 352–364. [[CrossRef](#)]
11. Bringi, V.N.; Chandrasekar, V. *Polarimetric Doppler Weather Radar: Principles and Applications*; Cambridge University Press: Cambridge, UK; New York, NY, USA, 2001; ISBN 0-521-62384-7.
12. Gorgucci, E.; Chandrasekar, V.; Bringi, V.N.; Scarchilli, G. Estimation of raindrop size distribution parameters from polarimetric radar measurements. *J. Atmos. Sci.* **2002**, *59*, 2373–2384. [[CrossRef](#)]
13. Brandes, E.A.; Zhang, G.; Vivekanandan, J. Drop size distribution retrieval with polarimetric radar: Model and application. *J. Appl. Meteorol.* **2004**, *43*, 461–475. [[CrossRef](#)]
14. Thurai, M.; Bringi, V.N.N.; Carey, L.D.D.; Gatlin, P.; Schultz, E.; Petersen, W.A.A. Estimating the Accuracy of Polarimetric Radar-Based Retrievals of Drop-Size Distribution Parameters and Rain Rate: An Application of Error Variance Separation Using Radar-Derived Spatial Correlations. *J. Hydrometeorol.* **2012**, *13*, 1066–1079. [[CrossRef](#)]
15. Ulbrich, C.W. Natural Variations in the Analytical Form of the Raindrop Size Distribution. *J. Clim. Appl. Meteorol.* **1983**, *22*, 1764–1775. [[CrossRef](#)]
16. Illingworth, A.J.; Blackman, T.M. The need to represent raindrop size spectra as normalized gamma distributions for the interpretation of polarization radar observations. *J. Appl. Meteorol.* **2002**, *41*, 286–297. [[CrossRef](#)]
17. Tokay, A.; D’Adderio, L.P.; Wolff, D.B.; Petersen, W.A. Development and Evaluation of the Raindrop Size Distribution Parameters for the NASA Global Precipitation Measurement Mission Ground Validation Program. *J. Atmos. Ocean. Technol.* **2020**, *37*, 115–128. [[CrossRef](#)]
18. Petersen, W.A.; Kirstetter, P.-E.; Wang, J.; Wolff, D.B.; Tokay, A. The GPM Ground Validation Program. In *Satellite Precipitation Measurement*; Levizzani, V., Kidd, C., Kirschbaum, D., Kummerow, C., Nakamura, K., Turk, F.J., Eds.; Springer Nature: Cham, Switzerland, 2020; pp. 471–502. ISBN 978-3-030-35798-6.
19. Petersen, W.A.; Krajewski, W.F. Status update on the GPM Ground Validation Iowa Flood Studies (IFloodS) field experiment. In Proceedings of the European Geosciences Union General Assembly, Vienna, Austria, 7–12 April 2013; European Geosciences Union: Vienna, Austria.
20. Barros, A.P.; Petersen, W.A.; Schwaller, M.R.; Cifelli, R.; Mahoney, K.; Peters-Lidard, C.D.; Shepherd, M.; Nesbitt, S.W.; Wolff, D.B.; Heymsfield, G.M.; et al. *NASA GPM-Ground Validation: Integrated Precipitation and Hydrology Experiment 2014 Science Plan*; Duke University: Durham, NC, USA, 2014.
21. Skofronick-Jackson, G.; Hudak, D.; Petersen, W.; Nesbitt, S.W.; Chandrasekar, V.; Durden, S.; Gleicher, K.J.; Huang, G.-J.; Joe, P.; Kollias, P.; et al. Global Precipitation Measurement Cold Season Precipitation Experiment (GCPEX): For Measurement’s Sake, Let It Snow. *Bull. Am. Meteorol. Soc.* **2015**, *96*, 1719–1741. [[CrossRef](#)]
22. Jensen, M.P.; Petersen, W.A.; Bansemmer, A.; Bharadwaj, N.; Carey, L.D.; Cecil, D.J.; Collis, S.M.; Del Genio, A.D.; Dolan, B.; Gerlach, J.; et al. The Midlatitude Continental Convective Clouds Experiment (MC3E). *Bull. Am. Meteorol. Soc.* **2016**, *97*, 1667–1686. [[CrossRef](#)]
23. Houze, R.A.; McMurdie, L.A.; Petersen, W.A.; Schwaller, M.R.; Baccus, W.; Lundquist, J.D.; Mass, C.F.; Nijssen, B.; Rutledge, S.A.; Hudak, D.R.; et al. The Olympic Mountains Experiment (OLYMPEX). *Bull. Am. Meteorol. Soc.* **2017**, *98*, 2167–2188. [[CrossRef](#)]
24. Thurai, M.; Gatlin, P.; Bringi, V.N.; Petersen, W.; Kennedy, P.; Notaroš, B.; Carey, L. Toward Completing the Raindrop Size Spectrum: Case Studies Involving 2D-Video Disdrometer, Droplet Spectrometer, and Polarimetric Radar Measurements. *J. Appl. Meteorol. Climatol.* **2017**, *56*, 877–896. [[CrossRef](#)]
25. Schwaller, M.R.; Morris, K.R. A Ground Validation Network for the Global Precipitation Measurement Mission. *J. Atmos. Ocean. Technol.* **2011**, *28*, 301–319. [[CrossRef](#)]
26. Ansari, S.; Del Greco, S.; Kearns, E.; Brown, O.; Wilkins, S.; Ramamurthy, M.; Weber, J.; May, R.; Sundwall, J.; Layton, J.; et al. Unlocking the Potential of NEXRAD Data through NOAA’s Big Data Partnership. *Bull. Am. Meteorol. Soc.* **2018**, *99*, 189–204. [[CrossRef](#)]
27. Marks, D.A.; Wolff, D.B.; Carey, L.D.; Tokay, A. Quality Control and Calibration of the Dual-Polarization Radar at Kwajalein, RMI. *J. Atmos. Ocean. Technol.* **2011**, *28*, 181–196. [[CrossRef](#)]

28. Gerlach, J.; Petersen, W.A. The NASA transportable S-band dual-polarimetric radar. Antenna system upgrades, performance and deployment during MC3E. In Proceedings of the 35th Conference on Radar Meteorology, Pittsburgh, PA, USA, 26–30 September 2011; American Meteorological Society: Pittsburgh, PA, USA; p. P192.
29. Brunkow, D.; Bringi, V.N.; Kennedy, P.C.; Rutledge, S.A.; Chandrasekar, V.; Mueller, E.A.; Bowie, R.K. A Description of the CSU–CHILL National Radar Facility. *J. Atmos. Ocean. Technol.* **2000**, *17*, 1596–1608. [[CrossRef](#)]
30. Petersen, W.A.; Knupp, K.R. Coauthors The UAH-NSSTC/WHNT ARMOR C-band dual-polarimetric radar: A unique collaboration in research, education and technology transfer. In *Proceedings of the 32nd Conference on Radar Meteorology*; Amer. Meteor. Soc.: Albuquerque, NM, USA, 2005; p. 12R.4.
31. Keenan, T.; Glasson, K.; Cummings, F.; Bird, T.S.; Keeler, J.; Lutz, J. The BMRC/NCAR C-Band Polarimetric (C-POL) Radar System. *J. Atmos. Ocean. Technol.* **1998**, *15*, 871–886. [[CrossRef](#)]
32. Tabary, P.; Augros, C.; Champeaux, J.-L.; Chèze, J.-L.; Faure, D.; Idziorek, D.; Lorandel, R.; Urban, B.; Vogt, V. Le réseau et les produits radars de Météo-France. *La Météorologie* **2013**, *8*, 15. [[CrossRef](#)]
33. Benjamin, S.G.; Weygandt, S.S.; Brown, J.M.; Hu, M.; Alexander, C.R.; Smirnova, T.G.; Olson, J.B.; James, E.P.; Dowell, D.C.; Grell, G.A.; et al. A North American Hourly Assimilation and Model Forecast Cycle: The Rapid Refresh. *Mon. Weather Rev.* **2016**, *144*, 1669–1694. [[CrossRef](#)]
34. Yang, F.; Pan, H.-L.; Krueger, S.K.; Moorthi, S.; Lord, S.J. Evaluation of the NCEP Global Forecast System at the ARM SGP Site. *Mon. Weather Rev.* **2006**, *134*, 3668–3690. [[CrossRef](#)]
35. Bleck, R.; Benjamin, S.; Lee, J.; MacDonald, A.E. On the Use of an Adaptive, Hybrid-Isentropic Vertical Coordinate in Global Atmospheric Modeling. *Mon. Weather Rev.* **2010**, *138*, 2188–2210. [[CrossRef](#)]
36. Dolan, B.; Rutledge, S.A.; Lim, S.; Chandrasekar, V.; Thurai, M. A Robust C-Band Hydrometeor Identification Algorithm and Application to a Long-Term Polarimetric Radar Dataset. *J. Appl. Meteorol. Climatol.* **2013**, *52*, 2162–2186. [[CrossRef](#)]
37. Stocker, E.F. GPM precipitation processing system. In *Proceedings of the Proc. SPIE 5234, Sensors, Systems, and Next-Generation Satellites VII*; Meynart, R., Neeck, S.P., Shimoda, H., Lurie, J.B., Aten, M.L., Eds.; SPIE: Barcelona, Spain, 2004; p. 13.
38. Pippitt, J.; Wolff, D.B.; Petersen, W.A.; Marks, D.A. Data and operational processing for NASA’s GPM Ground Validation program. In *Proceedings of the 37th Radar Conference on Radar Meteorology*; American Meteorological Society: Norman, OK, USA, 2015.
39. Silberstein, D.S.; Wolff, D.B.; Marks, D.A.; Atlas, D.; Pippitt, J.L. Ground Clutter as a Monitor of Radar Stability at Kwajalein, RMI. *J. Atmos. Ocean. Technol.* **2008**, *25*, 2037–2045. [[CrossRef](#)]
40. Wolff, D.B.; Marks, D.A.; Petersen, W.A. General Application of the Relative Calibration Adjustment (RCA) Technique for Monitoring and Correcting Radar Reflectivity Calibration. *J. Atmos. Ocean. Technol.* **2015**, *32*, 496–506. [[CrossRef](#)]
41. Scarchilli, G.; Gorgucci, E.; Chandrasekar, V.; Dobaie, A. Self-consistency of polarization diversity measurement of rainfall. *Geosci. Remote Sensing IEEE Trans.* **1996**, *34*, 22–26. [[CrossRef](#)]
42. Gorgucci, E.; Scarchilli, G.; Chandrasekar, V. A procedure to calibrate multiparameter weather radar using properties of the rain medium. *IEEE Trans. Geosci. Remote Sens.* **1999**, *37*, 269–276. [[CrossRef](#)]
43. Wang, Y.; Chandrasekar, V. Algorithm for Estimation of the Specific Differential Phase. *J. Atmos. Ocean. Technol.* **2009**, *26*, 2565–2578. [[CrossRef](#)]
44. Lee, G.W.; Zawadzki, I. Variability of Drop Size Distributions: Time-Scale Dependence of the Variability and Its Effects on Rain Estimation. *J. Appl. Meteorol. Climatol.* **2005**, *44*, 241–255. [[CrossRef](#)]
45. Cunningham, J.G.; Zittel, W.D.; Lee, R.R.; Ice, L.; Hoban, N.P. Methods for identifying systematic differential reflectivity (ZDR) biases on the operational WSR-88D network. In *Proceedings of the 36th Conference on Radar Meteorology*; American Meteorological Society: Breckenridge, CO, USA, 2013; p. 9B.5.
46. Iguchi, T.; Seto, S.; Meneghini, R.; Yoshida, N.; Awaka, J.; Le, M.; Chandrasekar, V.; Brodzik, S.; Kubota, T. *GPM/DPR Level-2 Algorithm Theoretical Basis Document Version 6*; NASA Goddard Space Flight Center: Greenbelt, MA, USA, 2018.
47. Seto, S.; Iguchi, T.; Oki, T. The Basic Performance of a Precipitation Retrieval Algorithm for the Global Precipitation Measurement Mission’s Single/Dual-Frequency Radar Measurements. *IEEE Trans. Geosci. Remote Sens.* **2013**, *51*, 5239–5251. [[CrossRef](#)]

48. Olson, W.S.; Team, G.C.R.-R.A. *GPM Combined Radar-Radiometer Precipitation Algorithm Theoretical Basis Document (Version 5)*; NASA Goddard Space Flight Center: Greenbelt, MA, USA, 2018.
49. Grecu, M.; Olson, W.S.; Munchak, S.J.; Ringerud, S.; Liao, L.; Haddad, Z.; Kelley, B.L.; McLaughlin, S.F. The GPM Combined Algorithm. *J. Atmos. Ocean. Technol.* **2016**, *33*, 2225–2245. [[CrossRef](#)]
50. Skofronick-Jackson, G.; Petersen, W.A.; Berg, W.; Kidd, C.; Stocker, E.F.; Kirschbaum, D.B.; Kakar, R.; Braun, S.A.; Huffman, G.J.; Iguchi, T.; et al. The Global Precipitation Measurement (GPM) Mission for Science and Society. *Bull. Am. Meteorol. Soc.* **2017**, *98*, 1679–1695. [[CrossRef](#)]
51. Dolan, B.; Fuchs, B.; Rutledge, S.A.; Barnes, E.A.; Thompson, E.J. Primary Modes of Global Drop Size Distributions. *J. Atmos. Sci.* **2018**, *75*, 1453–1476. [[CrossRef](#)]
52. Gatlin, P.N.; Thurai, M.; Bringi, V.N.; Petersen, W.; Wolff, D.; Tokay, A.; Carey, L.; Wingo, M. Searching for Large Raindrops: A Global Summary of Two-Dimensional Video Disdrometer Observations. *J. Appl. Meteorol. Climatol.* **2015**, *54*, 1069–1089. [[CrossRef](#)]
53. Battaglia, A.; Tanelli, S.; Mroz, K.; Tridon, F. Multiple scattering in observations of the GPM dual-frequency precipitation radar: Evidence and impact on retrievals. *J. Geophys. Res. Atmos.* **2015**, *120*, 4090–4101. [[CrossRef](#)]
54. Tanelli, S.; Sacco, G.F.; Durden, S.L.; Haddad, Z.S. *Impact of Non-Uniform Beam Filling on Spaceborne Cloud and Precipitation Radar Retrieval Algorithms.*; Hayasaka, T., Nakamura, K., Im, E., Eds.; International Society for Optics and Photonics: Kyoto, Japan, 2012; Volume 8523, p. 852308.
55. Seto, S.; Shimozuma, T.; Iguchi, T.; Kozu, T. Spatial and temporal variations of mass-weighted mean diameter estimated by GPM/DPR. In Proceedings of the 2016 IEEE International Geoscience and Remote Sensing Symposium (IGARSS), Beijing, China, 10–15 July 2016; IEEE: pp. 3938–3940.
56. Liao, L.; Meneghini, R. Physical Evaluation of GPM DPR Single- and Dual-Wavelength Algorithms. *J. Atmos. Ocean. Technol.* **2019**, *36*, 883–902. [[CrossRef](#)]
57. Battaglia, A.; Tanelli, S.; Kobayashi, S.; Zrnica, D.; Hogan, R.J.; Simmer, C. Multiple-scattering in radar systems: A review. *J. Quant. Spectrosc. Radiat. Transf.* **2010**, *111*, 917–947. [[CrossRef](#)]
58. Liao, L.; Meneghini, R.; Iguchi, T.; Tokay, A. Characteristics of DSD bulk parameters: Implication for radar rain retrieval. *Atmosphere (Basel)* **2020**, *11*, 670. [[CrossRef](#)]
59. Beck, J.; Berendes, T.; Gatlin, P.N.; LeRoy, A.; Stano, G.T. CAPRI: Cloud-based Analytic Framework for Precipitation Research. In *Proceedings of the Earth Science Technology Forum: Virtual*; NASA: Washington, DC, USA, 2020.
60. Shapiro, A.; Potvin, C.K.; Gao, J. Use of a Vertical Vorticity Equation in Variational Dual-Doppler Wind Analysis. *J. Atmos. Ocean. Technol.* **2009**, *26*, 2089–2106. [[CrossRef](#)]
61. Potvin, C.K.; Shapiro, A.; Xue, M. Impact of a Vertical Vorticity Constraint in Variational Dual-Doppler Wind Analysis: Tests with Real and Simulated Supercell Data. *J. Atmos. Ocean. Technol.* **2012**, *29*, 32–49. [[CrossRef](#)]
62. Jackson, R.; Collis, S.; Lang, T.J.; Potvin, C.K.; Munson, T. PyDDA: A Pythonic Direct Data Assimilation framework for wind retrievals (Version 0.5.2). *Zendo* **2020**. [[CrossRef](#)]
63. Petersen, W.A.; Gatlin, P.N.; Berendes, T.; Pippitt, J.L.; Munchak, S.J.; Wolff, D.B.; Marks, D.A. The GPM Validation Network Database: A multi-perspective tool for precipitation science. In *Proceedings of the American Geophysical Union Fall Meeting*; American Geophysical Union: San Francisco, CA, USA, 2019; p. H13P-1977.

